Three-Phase Three-Port Microinverter with Integrated Battery

Felipe C. Brandão [*] **Deyvid V. Souza** [**] **Bartolomeu F. dos Santos** [***]
Walbermark M. dos Santos [****]

[*] *Departamento de Engenharia Elétrica, Universidade Federal do Espírito Santo, ES, (e-mail: felipe.c.brandao@edu.ufes.br).*
[**] *Departamento de Engenharia Elétrica, Universidade Federal do Espírito Santo, ES, (e-mail: deyvid.souza@edu.ufes.br).*
[***] *Departamento de Engenharia Elétrica, Universidade Federal do Piauí, PI, (e-mail: bartolomeuf@ufpi.edu.br).*
[****] *Departamento de Engenharia Elétrica, Universidade Federal do Espírito Santo, ES, (e-mail: walbermark.santos@ufes.br)*

Abstract: This paper presents a dual-stage three-port microinverter for three-phase grid-connected PV applications with a battery connected in the third port. The battery operates as a backup power source to compensate for the power mismatch between the source and the grid and to store excess power generated by the PV panel. A DAB converter is used to provide galvanic isolation and maximum power point tracking of the PV panel. To verify the theoretical analysis of the proposed topology, a 400 W three-port microinverter was designed and simulated.

Keywords: microinverter, PV application, DAB converter, deadbeat control, grid-connected, energy storage

1. INTRODUCTION

Solar energy systems have experienced a rapid development in the last decade with a expanding focus on distributed generation (DG) due to the pursuit of costumers to decrease the cost of electricity. Brazil has surpassed the mark of 10GW of power from DG in 2022, with 4GW being installed on 2021 alone, ANEEL (2022).

Harnessing solar energy and converting it to electricity is mainly done by photovoltaic (PV) panels, which delivers a direct current, therefore, a inverter is necessary to deliver this energy to the usual power grid. By cost, the ideal solution would be to connect all the PV panels onto a single central inverter. Although, if any panel gets shaded, the power delivered by the system will be compromised. One solution would be the use of DC-DC converters connected to each panel, which would be responsible extract the optimum power from each one, and connected between each other in a single DC bus and the central inverter. However, this solution isn't robust in case of inverter failure, as there is no alternative path for power transfer to the grid. To solve this, one could use one inverter for each string of panels, so in case of failure, only the failed string would be removed, but the necessity of DC-DC converters to guarantee maximum power-point tracking (MPPT) remains.

It's still possible to take one step further and make the system "plug-and-play", by implementing the concept of microinverters, where each PV panel is individually connected to a single inverter, and thus, the maximum available power is guaranteed even in case of failure of any panel and the system becomes fully scalable, as to increase the power output is just needed to connect a new panel plus inverter set. This type of design was first introduced in the early 90's by the name of OK4 (Oldenkamp and de Jong (1998)). The microinverter market is expected to grow 14% during the forecast period of 2021 - 2026 according to IMARC (2021).

The amount of energy produced by solar cells are naturally intermittent, it varies with the angle between the sun and the PV panel and the radiation intensity, which, in turn, varies significantly with weather conditions. In addition, the peak power output of the PV panel will be, normally, at noon, which is often not the peak time for on-site needs. All that power variation would have to be balanced by the grid connected with the solar energy system. That can lead to extras costs as fees for power grid utilization and other issues such as instabilities in the grid. The integration of batteries allows to accommodate these uncertainties, by delivering power when the solar input is not available or storing the additional power generated at peak times. Thus, providing a reliable power flow to the consumers and other ancillary functions as peak-shaving.

Most of proposed topologies in literature and available commercially are of microinverters without integrated energy storage as shown by Hasan et al. (2017), Alluhaybi and Batarseh (2018) and Yuan et al. (2019), but the recent developments in battery technology and cost paved the way to increased academic and industrial interest in integration. Batarseh and Alluhaybi (2020) presents a review of a few examples of single stage microinverters with integrated battery.

In terms of desired characteristics, the microinverter needs to have high power density, to be installed together with the PV panel, high efficiency, to lose as little power as possible, and, preferably, galvanic isolation between the PV panel and grid for safety concerns. The Dual Active Bridge (DAB) converter, which was first discussed by De Doncker et al. (1991) and Kheraluwala et al. (1992) for aerospace applications, can fulfill all this requirements. It provides galvanic isolation with a high frequency transformer, which can also provide voltage boosting for the PV panel, it has bidirectional power flow, high power density, intrinsic protection against short-circuits, as its power flow goes to zero if the voltage in any side of the converter is short-circuited and, with the right conditions, high efficiency with soft switching.

Marei et al. (2015) proposes a microinverter based on the DAB converter which also executes the MPPT for the PV panel by controlling the PV voltage. This paper further expand this idea by the addition of a integrated battery in a three-port microinverter and proposes a control strategy for the voltages of the DAB converter to guarantee its soft-switching feature. This new configuration will allow to circumvent the main disadvantage of the DAB converter, the switching losses due to high number of components, and, at the same time, add more reliability to the microinverter. As the power efficiency of the inverter can change drastically with its load, the integration of a battery allows for the inverter to maintain operation closer to its optimum power point.

In section 2 the proposed topology will be detailed, in section 3, the simulation results are presented and a brief conclusion is presented on section 4.

2. PROPOSED TOPOLOGY

The proposed topology is illustrated in Figure 1. It consists of a three port device, with two ports on the low voltage side of the DAB converter for the PV panel and battery, and one port on the high voltage side for the grid-tied inverter.

The DAB converter provides the MPPT for the PV panel by controlling the voltage on the panel, through a perturb and observe (P&O) algorithm, it varies the voltage on the panel so the PV panel can deliver the optimum available power output. The DAB converter also inherently allows for bidirectional power flow, that way, the battery, which is connected through a bidirectional boost, can be charged either by the PV Panel or the grid, if necessary.

Due to the topology of the dual stage microinverter, the type of inverter connected to the high voltage side of the DAB can be freely chosen. The inverter will be responsible for controlling the dc-link voltage with the DAB converter. For this topology, the three-phase two-level inverter was chosen, for it allows for a better power quality output to the grid, without increasing too much the amount of components.

2.1 DAB Converter and control

High frequency switching is required to increase the power density on the converter, however, this would normally result on increased switching losses. As one requirement for microinverters is high efficiency, soft-switching techniques are required. The DAB converter was chosen primarily because, even though it requires eight switches to operate, it can achieve soft-switching (Zero Voltage Switching - ZVS) intrinsically to its operation and has the higher power density among other isolated topologies.

To simplify the control of the DAB converter, the phase-shift modulation is used, as it effectively only needs one command signal for the primary (high voltage or inverter's side) and one for the secondary (low voltage or PV panel's side) of the converter. The control variable is the phase angle difference (ϕ) between the command signals of the bridges, which will be used to generate the control signals of the switches and control the voltage over the PV panel and, consequently, control the power flow in the converter while the duty ratio remains constant at 50%.

The DAB converter can be viewed as two square waves sources associated by a inductance. Figure 3 shows the square waves, where V_i and V_o are the input and output voltages, respectively, and the resulting current in the inductance (I_L). With this, it's possible to find the the mean output or input current and, with it, the equation for the output power (1).

$$P_o = \frac{V_i V_o \phi_N}{N \omega_D L_{lk}} \left(1 - \frac{|\phi_N|}{\pi}\right) \tag{1}$$

where ω_D is the switching angular frequency, ϕ_N is the nominal phase-shift, L_{lk} is the leakage inductance and N is the turn ratio of the transformer, given by eq. 2.

$$N = \frac{V_o}{V_i d} \tag{2}$$

where d is the transformation ratio, which gives the relation between the turn ratio and the actual voltages applied in the converters terminal.

As explained by Kirsten et al. (2014), by analyzing the inductance's current waveform in Figure 3, it's possible to identify two transitions points, I_x and I_y, which are given by eq. 3 and eq. 4. The ZVS will happen when I_x and I_y are greater than zero. By plotting the output power for this condition as a function of the phase-shift angle, we can see the limits in which the ZVS is guaranteed.

$$I_x = \frac{V_i}{\omega_D L_{lk}} \frac{[2\phi d - \pi(d-1)]}{2} \tag{3}$$

$$I_y = \frac{V_i}{\omega_D L_{lk}} \frac{[2\phi + \pi(d-1)]}{2} \tag{4}$$

From Figure 4 it's possible to see that the soft switching can be lost while operating with low power, which leads to a substantial increase in switching losses in the converter. This effect is even more significant when the voltage ratio between primary and secondary side mismatches the transformer turn ratio. As the DAB's function is to perform the MPPT algorithm, if the inverter's side voltage remained constant, the voltages would rarely be matched exactly in the transformer, and the converter would loose its soft switching characteristic. To counteract this effect,

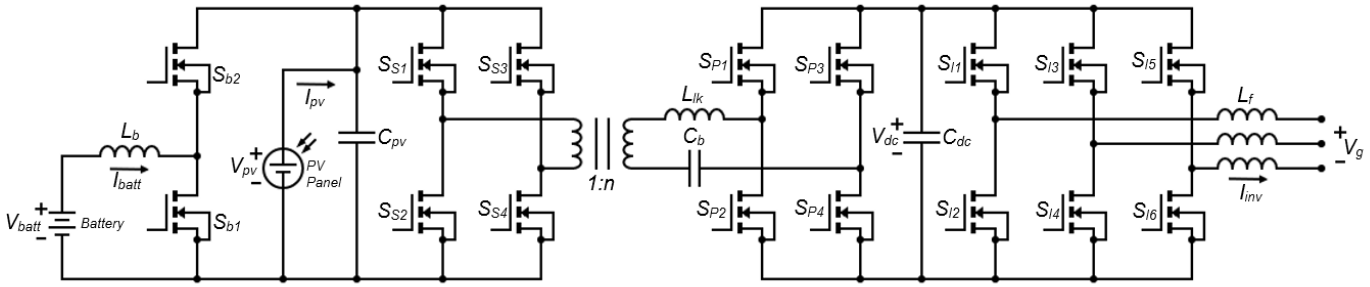

Figure 1. Proposed topology

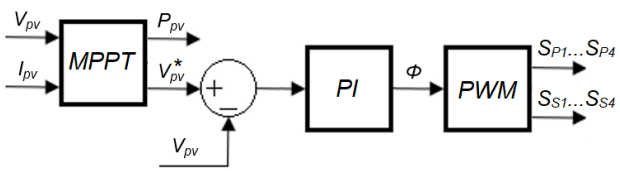

Figure 2. DAB control scheme

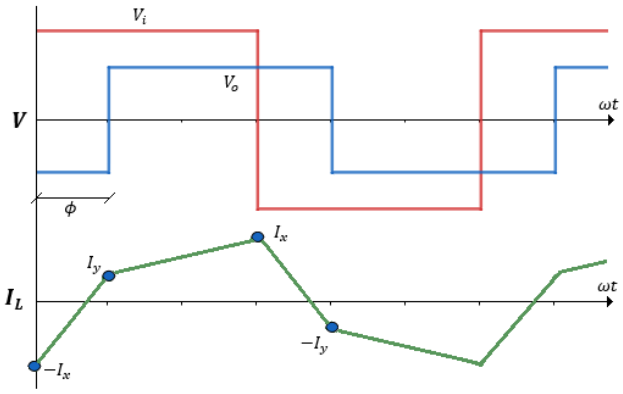

Figure 3. Voltages and current waveform in the DAB converter

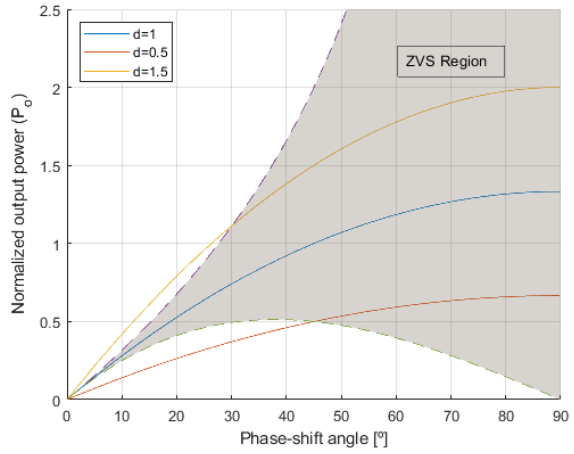

Figure 4. DAB's ZVS region

the reference voltage on the inverter's side will also have to be adjusted, so the primary and secondary voltages on the DAB converter remains in its ideal ratio.

By defining the main parameters of the converter, such as nominal power (P_{oN}), primary and secondary voltages (V_{dc} and V_{pv}, respectively), switching angular frequency (ω_D) and nominal phase-shift (ϕ_N), it's possible to adjust the values of the components of the converter: the transformer, the leakage inductance and the input and output capacitors.

The turn ratio of the transformer is given by the relation between the primary and secondary voltages using eq. 2, with the transformation ratio (d) being kept equal to 1, to operate in the ZVS region of the converter.

The leakage inductance is given by eq. 5, which is directly given by the output power equation.

$$L_{lk} = \frac{V_{dc} V_{pv} \phi_N}{N \omega_D P_{oN}} \left(1 - \frac{|\phi_N|}{\pi}\right) \tag{5}$$

Lastly, the capacitors are give by eq. 6.

$$C_{dc} > \frac{\phi_N P_{oN}}{\omega_s V_{dc}^2 \Delta V_{dc\%}} \tag{6}$$

where $\Delta V_{dc\%}$ is the percentage oscillation in the bus voltage. The same equation is used to the capacitor on the PV side, just changing the respective voltage.

A blocking capacitor is also used to avoid saturation of the transformer, and it's chosen by selecting a sufficiently high value to avoid resonances in the converter.

2.2 Boost Converter and control

The battery is connected to PV side of the DAB converter through a bidirectional boost. The battery acts as a support to the microinverter to provide a constant power output. It will provide the necessary power to compensate when the PV panel isn't able due to weather conditions, and will absorb the excess energy when the extra power isn't needed. The battery's state of charge (SoC) is monitored to control when the battery can provide power.

The boost's control reads the PV power from the MPPT algorithm, and uses it to regulate how much power the battery has to provide. The power reference is fed into a PI controller to get the duty ratio of the boost converter and, with a PWM, delivers the signals for the boost switches.

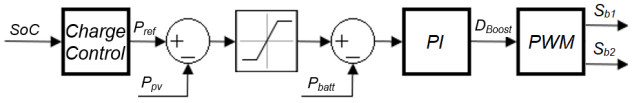

Figure 5. Boost control scheme

2.3 Tree-phase inverter and control

A conventional two-level three phase inverter was chosen, it is bidirectional and can provide power with low harmonic distortion to the grid with a simple L filter. The inverter has three legs with two switches on each. To avoid short-circuits, the switches operates with complementary activation on each leg, when one is turned on, the other should be turned off.

As discussed, its main function will be to control the voltage on the DC-link with the DAB converter and it will get the voltage reference value directly from the MPPT algorithm so as to keep the voltages across the DAB transformer matched with its turn ratio. But the DC-link voltage can't decrease or increase in all range of the MPPT algorithm, due to the maximum voltage on transistors or minimum voltage to provide the necessary output voltage matching the grid. For this reason, a saturation is implemented in the voltage reference for the DC-Link. While inside the linear region, the DAB's voltages will remain matched with the transformer turn ratio, but if the MPPT algorithm deviate into the saturation zone, then the voltages will mismatch and the DAB converter might operate outside the ZVS region.

The DC-link voltage is controlled through a PI controller using a synchronous reference frame, or dq-coordinates, which gives as output the reference current (I_d^*) to a deadbeat current controller, which is a well-known predictive control method and has a fast dynamic response, but it's sensitive to model parameter variation. The deadbeat model is in a stationary reference frame, $\alpha\beta$-coordinates, this is done to avoid the coupling effects while working with dq-coordinates, which could create another point of mismatch between the system and the model if the grid frequency deviates from its nominal value.

The deadbeat controller uses a model for a grid-tied inverter that can be expressed in stationary reference frame as:

$$\frac{d\mathbf{I}}{dt} = -\frac{R_f}{L_f}\mathbf{I} + \frac{1}{L_f}(\mathbf{V} - \mathbf{V_g}) \tag{7}$$

where $\mathbf{I}$ is the inverter current, $\mathbf{V}$ is the inverter voltage before the filter and $\mathbf{V_g}$ is the grid voltage.

Using Euler method to discretize 7, it's possible to obtain the reference voltage value to obtain zero current error in the next sampling instant, as shown in 8.

$$\mathbf{V}^*(k) = \frac{L_f}{T_s}\left[\mathbf{I}^*(k+1) - \left(1 - \frac{R_f T_s}{L_f}\right)\mathbf{I}(k)\right] + \mathbf{V_g} \tag{8}$$

where T_s is the sampling time.

This value is used as input in a space vector modulation (SVM), which will output the command signals for the inverter switches.

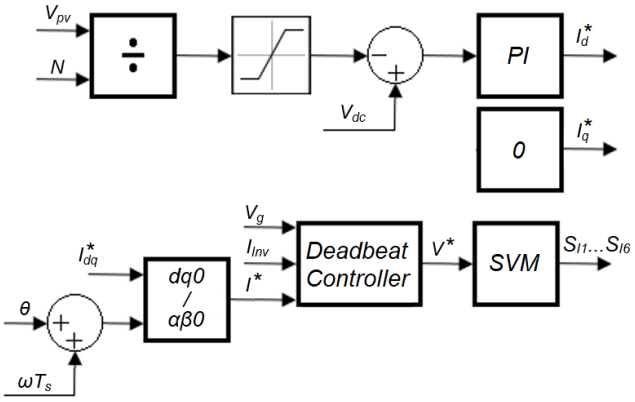

Figure 6. Inverter control scheme

The deadbeat controller is suited for this grid-tied inverter, because unlike in a inverter connected directly to a load, where the load impedance can vary drastically implying in a high margin of error in the deadbeat model, the model for a grid-tied inverter only takes the filter impedance into account, which isn't expected to deviate much from its nominal value. Also, the output power and, consequently, the current, is expected to remain relatively constant due to the integrated battery, which will also contribute to the stability of the control. The deadbeat controller can be negatively affected by the grid impedance, which could be addressed by using a LCL filter, but, for practical applications, this would make the microinverter bulkier, which isn't desired.

The reference current generated by the PI controlled is for the instant 'k' and the deadbeat controller needs the current for the instant 'k+1'. For that reason, the reference is adjusted by adding a factor of ωT_s to the phase angle θ obtained from a PLL block, while the transformation from dq-coordinates to $\alpha\beta$-coordinates of the reference current is being calculated.

Even though this type of Deadbeat control presents a steady-state error in stationary reference frame, this error will be compensated by the PI controller that is generating the reference current for the Deadbeat and the final controlled variable, the DC-link voltage, will still reach the desired value.

The values for the L filter are obtained by defining the maximum variation on current (ΔI) on the inverter output and its frequency.

$$L_f = \frac{V_{dc}}{8 f_I \Delta I} \tag{9}$$

3. SIMULATION RESULTS

To evaluate the effectiveness of the proposed topology, a model was implemented on Simulink R2018b. The system was subjected to varying irradiance and temperature to verify the model in different operating conditions, while maintaining the output power constant with the battery assistance. As a perfect match between the model and the real components used isn't achievable, a 10% difference is intentionally set in the model used by the deadbeat controller in respect to the actual components being simulated.

Table 1 show the parameters of the microinverter and the value for all the components used in the simulation. A Elgin half-cell PV panel is modeled, its parameter are shown on Table 2.

The microinverter will be connected to only one PV panel, for this reason its nominal power is limited to 400W. For computational restrictions, the DAB frequency is limited to 20kHz, but, in practical applications, it could be increased to higher frequencies, in the range of hundreds of kilohertz or higher.

Table 1. Parameters and Components

Parameter and Component	Symbol	Value
Boost Nominal Power	P_{Bo}	200 W
Battery Nominal Voltage	V_{Batt}	10 V
Boost Inductance	L_b	375 μH
Boost Inductance Resistance	R_b	3.75 mΩ
Boost Switching Frequency	f_B	20 kHz
Microinverter Output Power	P_{oN}	400 W
DAB Primary Voltage (grid side)	V_{dc}	533 V
DAB Secondary Voltage (PV side)	V_{pv}	40 V
DAB Switching Frequency	f_D	20 kHz
DAB Leakage Inductance	L_{lk}	3.3 mH
DAB Leakage Inductance Resistance	R_{lk}	33 mΩ
DAB Primary Capacitor	C_{dc}	5 μF
DAB Secondary Capacitor	C_{pv}	500 μF
DAB Blocking Capacitor	C_b	50 μF
Grid Line Voltage	V_{ll}	220 V
Grid Frequency	f_g	60 Hz
Inverter Switching Frequency	f_I	20 kHz
Filter Inductance	L_f	63.5 mH
Filter Inductance Resistance	R_f	635 mΩ

Table 2. PV panel parameters at STC

Parameter	Value
Nominal Power	450 W
Number of Cells	144
Open circuit Voltage	50.22 V
Short circuit Current	11.48 A
Voltage at MPP	41.40 V
Current at MPP	10.14 A

The first simulation starts with a irradiance of 1000 W/m^2 and 25 ^{o}C, at 0.66 seconds the irradiance is reduced to 600 W/m^2 and at 1.33 seconds the irradiance returns to 1000 W/m^2. The output power of the inverter is set at 350 W and the dynamic response of the system is evaluated.

Figure 7 shows the power output of the different segments of the converter, as can be seen the power output of the converter remains constant at the designed value, with the battery absorbing the excess power delivered by the PV panel in high irradiance state, and delivering the necessary power to complement the PV panel while the irradiance is low. The power spike in the inverter output is due to difference between the sampling time and the irradiance step time.

The boost converter adjusts the power output of the battery to keep the constant power of the microinverter.

Figures 9 and 10 shows the voltage on both sides of the DAB converter. As can be seen, the MPPT algorithm, changes the reference voltage on the to extract the maximum power from the PV Panel. The DC-link reference voltage is adjusted to keep the relation between both sides of the DAB converter as close as possible to the transformer ratio.

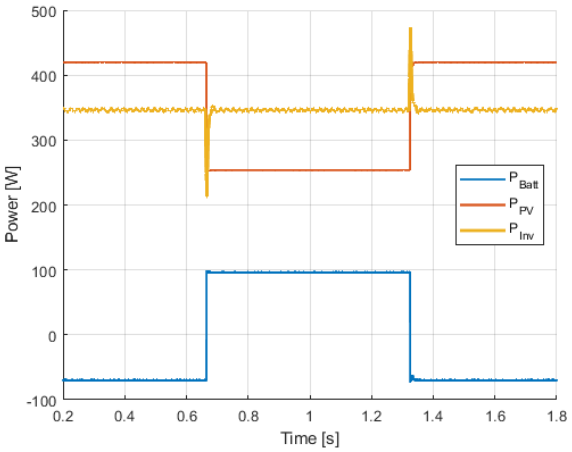

Figure 7. Powers across the microinverter with irradiance variation

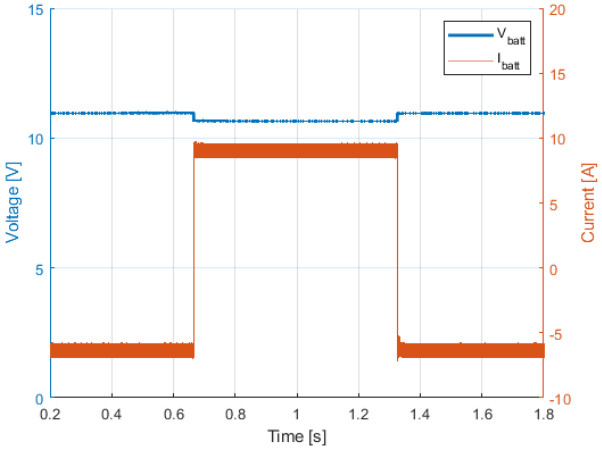

Figure 8. Battery voltage and current with irradiance variation

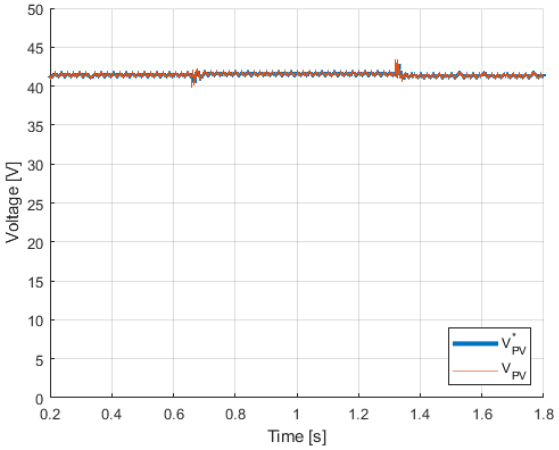

Figure 9. PV panel voltage with irradiance variation

Even with the difference between the model and the simulated components, the deadbeat controller was still

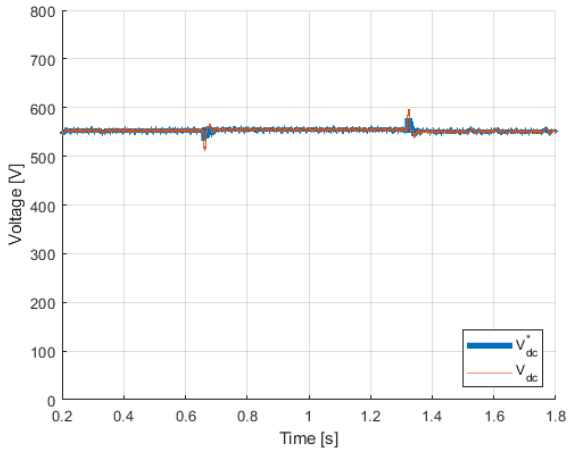

Figure 10. DC-link voltage with irradiance variation

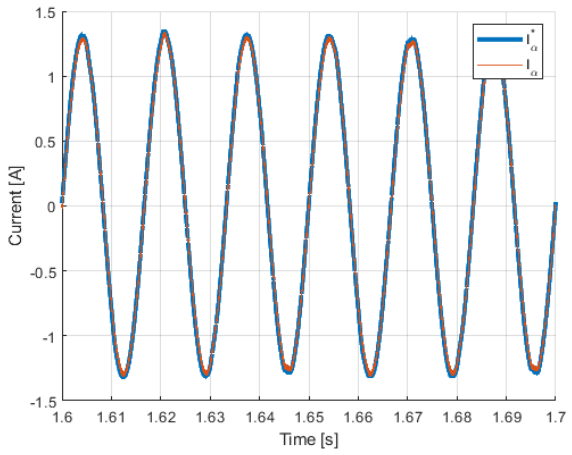

Figure 11. I_α component of Deadbeat Controller

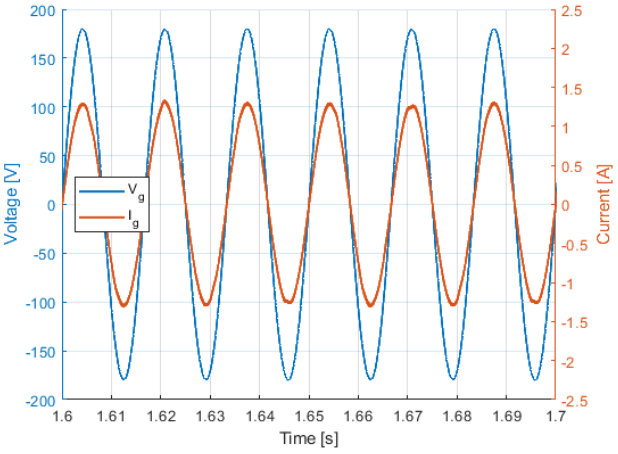

Figure 12. Grid voltage and current

able to provide a fast response with minimum error to the inverter as can be seen in Figure 11.

Figures 12 and 13 shows the voltage and current of the grid's phase 'A' delivered with unitary power factor and THD close to 1%.

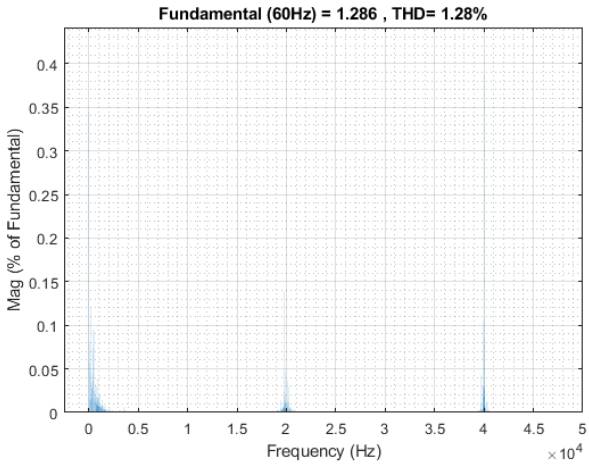

Figure 13. FFT analysis of grid current

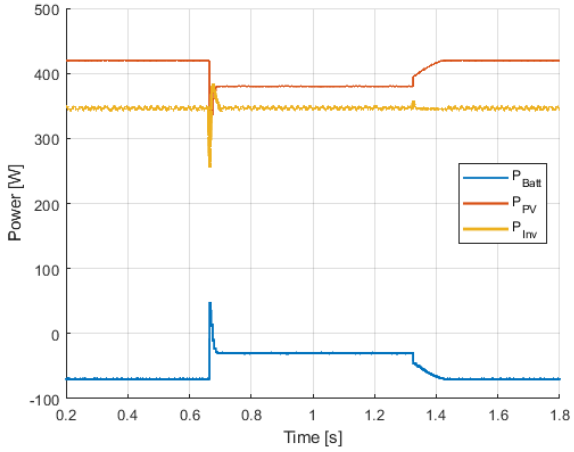

Figure 14. Powers across the microinverter with temperature variation

The simulation is repeated with variation of the PV panel's temperature. At 0.66 seconds the PV panel's temperature is increased by 30^{o}C and at 1.33 seconds the temperature returns to 25^{o}C. It's possible to see in Figure 14 that the power is maintained at the desired output value. Figure 15 shows the MPPT algorithm working, and the correlation between the V_{pv} and V_{dc} voltages to guarantee the soft-switching operation.

4. CONCLUSION

This paper presented a DAB based topology for a microinverter with a integrated battery. The battery enhances the capabilities of the microinverter, by making the power output more reliable and safer for the grid. A MPPT algorithm is used in conjunction with the DAB converter to control the PV panel voltage, while the DC-link voltage is controlled by the inverter, using a deadbeat controller. The PV panel and DC-link voltages are correlated by the transformer turn ratio to keep the DAB converter operating in the ZVS region. The proposed system is simulated using the Simulink R2018b platform and its dynamic response is evaluated. The results show that the microinverter is capable of delivering reliable power with

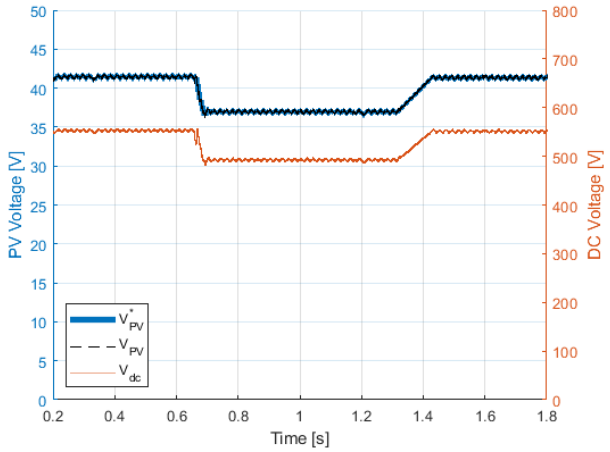

Figure 15. DAB voltages with temperature variations

a fast response. Even though the Deadbeat controller may present oscillations, they weren't significant in this work.

It is worth mentioning that for the way the inverter control was implemented in this work, it needs the grid to function properly, so it can't deliver power in case of grid interruption. A future work can evaluate the association of multiple microinverters with grid formation for 'no-grid' applications.

Future research can evaluate a detailed analysis of the microinverter's efficiency, its response with a more advanced battery model, to explore the multi-port characteristic of the microinverter with a variation of types of inverters and the capabilities to perform ancillaries functions as reactive power management and peak-shaving.

REFERENCES

Alluhaybi, K. and Batarseh, I. (2018). Review and comparison of single-phase grid-tied photovoltaic microinverters. In *2018 IEEE Energy Conversion Congress and Exposition (ECCE)*, 7101–7108. doi:10.1109/ECCE.2018.8558076.

ANEEL (2022). Brasil ultrapassa marca de 10 gw em micro e minigeração distribuída. `https://bit.ly/37bhyGa`, Last accessed on 2022-05-01.

Batarseh, I. and Alluhaybi, K. (2020). Emerging opportunities in distributed power electronics and battery integration: Setting the stage for an energy storage revolution. *IEEE Power Electronics Magazine*, 7(2), 22–32. doi:10.1109/MPEL.2020.2987114.

De Doncker, R., Divan, D., and Kheraluwala, M. (1991). A three-phase soft-switched high-power-density dc/dc converter for high-power applications. *IEEE Transactions on Industry Applications*, 27(1), 63–73. doi:10.1109/28.67533.

Hasan, R., Mekhilef, S., Seyedmahmoudian, M., and Horan, B. (2017). Grid-connected isolated pv microinverters: A review. *Renewable and Sustainable Energy Reviews*, 67, 1065–1080. doi:https://doi.org/10.1016/j.rser.2016.09.082. URL `https://www.sciencedirect.com/science/article/pii/S136403211630572X`.

IMARC (2021). Solar microinverter market: Global industry trends, share, size, growth, opportunity and forecast 2021-2026. Available at `https://www.imarcgroup.com/solar-microinverter-market/toc`.

Kheraluwala, M., Gascoigne, R., Divan, D., and Baumann, E. (1992). Performance characterization of a high-power dual active bridge dc-to-dc converter. *IEEE Transactions on Industry Applications*, 28(6), 1294–1301. doi:10.1109/28.175280.

Kirsten, A., Carloto, F., Oliveira, T., Roncalio, J., and Dalla Costa, M. (2014). Phase-shift design methodology for the dab converter. *Eletrônica de Potência*, 19, 231–240. doi:10.18618/REP.2014.3.231240.

Marei, I., El-Helw, H., and Al-Hasheem, M. (2015). A grid-connected pv interface system based on the dab-converter. In *2015 IEEE 15th International Conference on Environment and Electrical Engineering (EEEIC)*, 161–165. doi:10.1109/EEEIC.2015.7165534.

Oldenkamp, H. and de Jong, I. (1998). Next generation of ac-module inverters.

Yuan, J., Blaabjerg, F., Yang, Y., Sangwongwanich, A., and Shen, Y. (2019). An overview of photovoltaic microinverters: Topology, efficiency, and reliability. In *2019 IEEE 13th International Conference on Compatibility, Power Electronics and Power Engineering (CPE-POWERENG)*, 1–6. doi:10.1109/CPE.2019.8862334.